First experiences of photoacoustic imaging for detection of melanoma metastases in resected human lymph nodes

D. J. Grootendorst, MSc [1,*], J. Jose, PhD [1], M. W. Wouters, MD, PhD [1], H. van Boven, MD, PhD [2], J. Van der Hage, MD, PhD [2], T.G. Van Leeuwen, PhD [1,3], W. Steenbergen, PhD [1], S. Manohar, PhD [1], T. J. M. Ruers, MD, PhD [2,4]

[1] Biomedical Photonic Imaging Group, MIRA Institute for Biomedical Technology and Technical Medicine, Faculty of Science and Technology, University of Twente, P.O. Box 217, 7500 AE Enschede, The Netherlands

[2] Netherlands Cancer Institute - Antoni van Leeuwenhoek Hospital (NKI-AVL), P.O Box 90203, 1006 BE Amsterdam, The Netherlands

[3] Biomedical Engineering and Physics, Academic Medical Center, University of Amsterdam, P.O. Box 2270, 1100 DE Amsterdam, The Netherlands

[4] Nanobiophysics Group, MIRA Institute for Biomedical Technology and Technical Medicine, Faculty of Science and Technology, University of Twente, P.O. Box 217, 7500 AE Enschede, The Netherlands. Also at Netherlands Cancer Institute - Antoni van Leeuwenhoek Hospital (NKI-AVL), The Netherlands;

*Corresponding to: Diederik Grootendorst, MSc, Biomedical Photonic Imaging Group, P.O. Box 217, 7500 AE, Enschede, The Netherlands. Email: d.j.grootendorst@utwente.nl

Contract Grant Sponsor: PRESMITT project of the AgentschapNL program IOP Photonic Devices, Contract grant number: (IPD067771) and the Mira Institute for Biomedical Technology and Technical Medicine.

Dr. Van Leeuwen, Dr. Manohar and Dr. Steenbergen have a minor interest in PA Imaging bv, which however did not finance the research in any way.

Abstract

Background and objective: Excision and histological assessment of the first draining node (Sentinel Lymph Node) is a frequently used method to assess metastatic lymph node involvement related to cutaneous melanoma. Due to the time required for accurate histological assessment, nodal status is not immediately available to the surgeon. Hence, in case histological examination shows metastases, the patient has to be recalled to perform additional lymphadenectomy. To overcome these drawbacks we studied the applicability of photoacoustic tomographic imaging as an intra-operative modality for examining the status of resected lymph nodes.

Materials and Methods: In melanoma patients undergoing lymphadectomy for metastatic disease, six suspect lymph nodes were photoacoustically (PA) imaged using multiple wavelengths. Histopathologal examination showed three nodes without tumor cells (benign nodes) and three nodes with melanoma cells (malignant nodes). PA images were compared with histology and anatomical features were analyzed. In addition, PA spectral analysis was performed on areas of increased signal intensity.

Results: After correlation with histopathology, multiple areas containing melanoma cells could be identified in the PA images due to their increased response. Malignant nodes showed a higher PA response and responded differently to an increase in excitation wavelength than benign nodes. In addition, differences in anatomical features between the two groups were detected.

Conclusions: Photoacoustic detection of melanoma metastases based on their melanin content proves to be possible in resected human lymph nodes. The amount of PA signal and several specific anatomical features seem to provide additional characteristics for nodal analysis. However, it is as yet preliminary to designate a highly accurate parameter to distinguish between malignant and benign nodes. We expect to improve the specificity of the technique with a future implementation of an adjusted illumination scheme and depth correction for photon fluence.

Introduction

The incidence of melanoma is increasing faster than any other cancer, with about 68,000 new cases diagnosed every year in the United States (1). A similar number was diagnosed each year in Europe in 2008 (2). When diagnosed early and appropriately excised, melanoma is a curable malignancy. However, mortality is high for patients with advanced disease with 1-year survival rates of about 40% (3).

Early stage melanoma is primarily treated by a wide surgical excision of the primary tumor followed by a sentinel lymph node (SLN) biopsy if the Breslow thickness of the melanoma exceeds 1 mm (4). Combined histopathological and immunohistochemcial assessment of the excised SLN(s) proves to be an accurate predictor of the pathological status of nodal basin and as a result patient survival (5). Once metastases are detected in the SLN(s) surgical intervention is continued in the form of a radical lymphadenectomy of the regional lymph

node basin (5). Radical lymphadenectomy, however may lead to serious morbidity, such as lymphedema (2% to 18% of cases), pain (16% to 56%), impaired joint mobility (4% to 45%), and limb weakness (19% to 35%) and should therefore be avoided if no clinical reason is present (6).

The time required for histopathological preparation of the SLN is known to amount to 5 days (7) due to fixation and staining of the tissue. This implies that in case the SLN turns out to harbour tumor metastases, a second operation has to be scheduled for the additional lymphadenectomy. This two-step approach leads to additional patient discomfort, morbidity cost, and organizational distress (8). There is thus a requirement for an intra-operative nodal scanning technique to enable a fast analysis of the entire nodal volume, and ascertain metastatic involvement during the SLN procedure. A positive metastatic involvement of the SLN will directly lead to a lymphadenectomy, which can be carried out in the same session, avoiding the need for patient recall.

Photoacoustics (PA) is one of the techniques which has the potential to develop into such a fast intra-operative imaging modality. PA imaging relies on the detection of acoustic waves produced by the thermoelastic expansion of tissue following absorption of short pulsed laser illumination. This allows the mapping of endogenous tissue chromophores like hemoglobin and melanin (9,10) . PA retains a good spatial resolution at higher imaging depths compared to purely optical imaging, due to the decreased amount of ultrasound scattering in tissue (11-14). The components of a PA imaging system are relatively inexpensive compared to MRI and no ionizing radiation is required for image acquisition. Melanoma cells, harbouring high optical absorbing melanin particles, can thus potentially be detected using PA imaging without any additional labelling.

Several groups including our own have looked into various aspects of melanoma metastases detection using PA imaging. Nedosekin *et al* (15) showed with high speed photoacoustic flow cytometry that circulating human melanoma cells could be detected in real-time in a mouse model. Capturing of the circulating melanoma cells using magnetic or gold nanoparticle labelling has shown to further improve the sensitivity of this technique (16,17). McCormack *et al* (18) showed elevated PA responses in canine lymph nodes inserted with melanoma cells. Recently, we demonstrated that tomographic imaging of melanoma cells inside a pig lymph node using NIR illumination is possible, and spectral analysis could be used to support the visual discrimination of such deposits (19). Further, we performed the first PA studies on human lymph nodes and showed that nodal outline, shape and size could be determined with accuracy using 532 nm (20), and the PA response could be correlated to the presence of melanoma (19). However, before PA detection of melanoma metastases could be translated into a clinical setting, more information should be obtained on how to distinguish metastatic nodes from benign and hyperplastic nodes.

In this study, we present our experiences on the use of PA imaging for the detection of nodal melanoma metastases, based on the scans of six resected human lymph nodes. Three nodes were found to be benign and three malignant after histopathological analysis. PA images are correlated to histological sections and anatomical features are identified. The traditionally

described ultrasound morphologic features predictive of malignancy which are size >1 cm, a rounded shape and the absence of a notch with or without blood vessels (hilum) (21-23) are also taken into account. In addition, we analyse the use of multispectral imaging to distinguish malignant nodes from benign nodes and discuss some instrumental drawbacks of the present embodiment of this new approach. Eventually this knowledge should lead to the development of a new nodal analysis technique which could improve intra-operative decision making for sentinel lymph nodes.

Materials and Methods

Research Protocol

The experimental protocol to perform PA imaging of melanoma metastases in resected human lymph nodes was approved by the medical ethics committee of the Netherlands Cancer Institute (NKI). Patients were included into the study when they had to undergo a lymphadenectomy because of proven metastatic disease of the inguinal or axillary lymph node basin. In these patients lymphadenectomy was performed according to standard procedures. All patients consented to the approved protocol. After the lymphadenectomy procedure, one or two nodes were selected and excised for PA imaging. Nodes were selected without knowledge of their pathological status. The nodes were scanned photoacoustically and routine pathological examination was subsequently performed by slicing each node in half and obtaining one slice from each half. Before further slicing, both halves were photographed to obtain an overview of the interior of some of the nodes. Tissue was stained using a normal haematoxylin and eosin (H&E) stain. Of the total of 6 imaged lymph nodes, 3 nodes proved to contain metastatic cells (malignant) after pathological analysis and 3 were labelled as benign.

Setup

The photoacoustic setup employed has been described earlier in detail (19) and consists of a Q-switched Nd:YAG laser (Brilliant B, Quantel, France) with an optical parametric oscillator (Opotek, 700 to 950 nm) operating at a 10 Hz repetition rate. Radiant exposure on the surface of the sample could be varied up to 40 mJ/cm^2. Samples were placed inside an Agar holder (Fig. 1) and light was directed to fall on top of the sample using a beam expander. The produced acoustic signals are recorded with the help of a curvilinear detector array (Imasonic, Besançon) consisting of 32 elements. The piezo elements of the detector have a central frequency of 6.25 MHz with a receiving bandwidth greater than 80% which results in an in-plane resolution of around 150 µm and a slice thickness of around 1 mm (24). The array is placed to detect sound in a plane orthogonal to the light beam and it rotates around the object to acquire a tomographic measurement.

Imaging

Multispectral imaging can assist in the visualization of melanoma metastases due to differences in the optical absorption spectra of melanin and other biological chromophores like hemoglobin (19,25). We varied the illumination wavelength and obtained images of the resected nodes between 720 to 800 nm. In this range, hemoglobin shows a flat or increased

absorption depending on its state while melanin absorption decreases with increasing wavelength.

Five sectional PA images in depth of each resected node were acquired to obtain an overview of each node. The PA images around the central plane of the node, in the results referred to as PA slices, were used for comparison with histology because this plane is closest to the histological sections made. Nodal dimensions were calculated from the histological slides and the PA images. In addition, the PA images were visually analyzed with regard to their shape and the presence of a hilum. All nodes were imaged using several different excitation wavelengths as displayed in Table 2. Energy was varied depending on the size of the node in order to approach an equal fluence in moderate and thicker samples.

To quantify the amount of PA response at each illumination wavelength, we calculated the Average Pixel Values (APV) at selected regions of interest within the image. Regions of interest in the PA images were selected according to the amount of PA response and the results of histopathology. Interpolation was used for missing excitation wavelength information. Values of both benign and malignant nodes were normalized for the energy input (Table 2), plotted and compared.

Results

We present all results of the studied lymph nodes, subdivided according to dignity of the node, malignant (nodes 1-3) or benign (nodes 4-6), as known from histopathology. A combination of the PA images at 720 nm, histological, and overview photographs of the malignant and benign nodes is displayed in Figure 2 and 3. Table 1 displays the maximum diameter of each node measured in both the PA images and histopathology.

Imaging malignant lymph nodes

Node 1 features a darkened appearance and included some additional fat (Fig. 2D). The PA slice (Fig. 2B) obtained in the central plane at a depth of approximately 3 mm, shows a pronounced nodal outline which lacks a clear bean shape and appears more rounded. No clear hilum could be located. Most contrast is located in the nodal outline while most of the nodal interior shows low PA response. An area of increased response is located at two o'clock containing a diameter of 0.7 cm (green arrow). Pathology shows the presence of melanoma throughout the entire node with large quantities of melanin present in an area corresponding in dimension to the area of photoacoustic signal increase at two o'clock (Fig. 2C). The larger melanin deposits in the lower part of the node could not be retrieved within the PA map (blue arrow).

Node 2 showed no clear darkening after excision and contained only small quantities of extra nodal fat. The PA slice (Fig. 2F) in the nodal plane taken at a depth of 5 mm shows an increase in signal at different locations heterogeneously throughout the node with an exception of the nodal center. Surrounding the area lacking PA response (red arrow) is a small ring of increased signal. No clear nodal outline or hilum could be detected although nodal features seemed to be more rounded compared to the PA images of the benign nodes (Fig. 3A and 3G). The photograph of the sliced node taken before pathological analysis (Fig. 2H) shows diffuse darkening throughout the node together with a small dark ring surrounding a

large necrotic area in the center of the node (red arrow). Shape of both the dark ring and the light colored necrotic area, correlate to the area respectively containing and lacking photoacoustic response (red arrow). Pathology confirms the presence of viable melanoma cells in the periphery of the necrotic area. (Fig. 2G). The shape of the necrotic area correlates with both the photograph and the PA image.

Node 3 features some darkening throughout the entire nodal surface with some deposits of extranodal fat after excision. The PA slice (Fig. 2J) around the central plane obtained at a depth of 4 mm did show a traceable nodal outline and locations of increased signal intensity. Absence of a clear bean shaped outline proved hard to deduce and no hilum could be located. Absorption at all wavelengths was most pronounced at three o'clock corresponding with a relatively small area (blue arrow). The area located at three o'clock displays a pronounced triangular shape, lacking PA contrast in its center. The photograph taken before pathological analysis (Fig. 2L) shows a node which contains several areas of pronounced darkening primarily located from three to nine o'clock. Located at three o'clock is a small triangular area corresponding in location, shape and size with the area of increased signal intensity in the photoacoustic image (blue arrow). A curved ray like PA intensity pattern (Fig. 2J) is noted in the upper area of the node which resembles the curved ray like structures in the photograph (red arrows). The larger darkened area at six o'clock (green arrow) did not show up clearly in the PA images although some signal was detected at this location. Histology (Fig. 2K) confirms the presence of melanoma throughout the node with larger melanin deposits in the lower areas of the node. Especially the triangular location at three o'clock and larger areas around five and six o'clock seem to include large quantities of melanin. The upper region of the node contains two distinct necrotic areas (light purple staining) which still contain some viable melanoma cells in their center and outer rings. These patterns correspond with the curved ray like patterns of our photographs and the detectable PA rings at twelve o'clock (red arrow).

Imaging benign lymph nodes

Node 4 showed no significant discolouring and contained some accessory fat after excision (Fig. 3C). The PA slices taken in the central plane at a depth of 3 mm (Fig. 3A) show a well defined nodal outline which resembles a bean shape and shows a pronounced hilum at ten o'clock (blue arrow). A speckled high contrast area (green arrow) is located at twelve o'clock. Pathology shows that the node contains reactive changes, however, no malignant cells were present in the specimen (Fig. 3B).

Node 5 did not show any discolouring but showed significant quantities of accessory fat after excision (Fig. 3F). In the PA slice at the central plane (2 mm beneath the surface) (Fig. 3D) the nodal outline proved hard to distinguish and the nodal diameter could therefore not be determined with accuracy. In addition, no defined hilum could be located. Most signal is located in the centre of the image showing a diffuse speckle pattern (red arrow). Pathological examination shows reactive changes throughout the node with absence of malignant cells (Fig. 3E).

Node 6 showed some discolouring and contained minor deposits of accessory fat after excision. PA images show a distinct nodal outline which is bean shaped (Fig. 3G) and the inclusion of a hilum (blue arrow) can be located at four o'clock. PA response is located throughout the entire nodal volume, although fluctuations are present in some locations. The photograph taken before pathological analysis (Fig. 3I) shows a fatty dark node which contains a hilum at four o'clock (blue arrow). Pathological examination (Fig. 3H, 4C) reveals that the node contains some fatty deposits and includes a lot of red blood cells inside several vessels explaining the darkened color. Malignant cells are not observed.

Multispectral analysis

The added potential benefit of multiple wavelength illumination is shown in node 6 (Fig. 4). The images obtained at 800 nm show a vessel like structure leaving the nodal hilum which could not be visualized using 720 nm (Fig. 4A-B, red arrow). Pathological examination revealed the presence of a blood vessel at this location (Fig. 4D, red arrow). The response inside the vessel depicted in node 6 (Fig. 4B, red arrow) proved to be increased, pointing to the presence of oxidized hemoglobin, however this trend was not measured in the rest of the nodal volume.

Spectral analysis was performed on the areas within each node containing most pronounced PA responses. For node 1-3 these areas were respectively the area at two o'clock (green arrow), the ring around the necrotic center of the node containing viable melanoma cells (red arrow) and the area at three o'clock (blue arrow). For node 4-6, spectral analysis was respectively performed on the region at twelve o'clock (green arrow), the centre of the image (red arrow) and the entire area within the nodal outline.

Figure 5 displays the multiple wavelength response of the selected areas within the nodes and shows that the PA response in the selected regions within the malignant nodes is larger than those within the benign ones. All nodes show most PA signal at 720 nm but the measured APVs within the malignant nodes show a larger decrease up to 800 nm than those within the benign nodes. Although node 3 shows a higher APV than the benign nodes, its decrease in APV up to 800 nm is less pronounced compared to node 1 and 2.

Discussion and Conclusions

As shown by our PA scans of six human lymph nodes, detection of melanoma cells in resected human lymph nodes proves to be possible using photoacoustics. In all three malignant nodes an increased PA response in the images could be correlated to the presence of melanoma cells verified by histopathology. This is the first study on both malignant and benign resected human samples demonstrating differences in PA response. However, it should be noticed that not all metastatic areas detected on histology could be visualized with PA. This could be attributed to the biological diversity of the metastases and their melanin content or the lack of optical penetration due to the optical thickness of malignant tissue.

In our understanding, the latter contributes most to this decreased detection rate since the optical density of the melanin-rich (malignant) tissue impedes imaging more than 5 mm beneath the nodal surface. This is shown in the PA image of lymph node 1 where the nodal

outline is enhanced while the PA response in the center of the node is less pronounced. As the photographs of the malignant nodes show, their tissue is slightly discoloured and in node 1 even severely darkened which produces an increased optical density compared to normal or -reactive nodal tissue. An improved illumination scheme, providing light from different angles onto the nodal volume could be useful to ensure that sufficient optical energy reaches the inner parts of the node. At the moment these adjustments are implemented and evaluated. It has to be mentioned that our final application purpose of scanning resected nodes during surgery does not require the scanning of nodes larger than 1-1.5 cm because it is already relatively certain that they harbour metastases. Loss of sensitivity due to illumination problems is therefore less likely to arise once the technique is used within a patient population which contains less pronounced nodal metastases, such as sentinel lymph nodes.

In the benign cases, a PA response was also noted but these were considerably weaker than in the malignant nodes, as shown by the APV (Fig. 5). Most likely, this PA reponse can be attributed to the presence of hemoglobin which could be present in small vessels or haemorrhages throughout the nodes. Other biological components like collagen and fat show minor absorption in the NIR range (11), and are therefore not suspected of generating this amount of response. In addition, during surgical resection of the lymph nodes, small blood vessels in the extranodal fat of the node may be disrupted causing little haemorrhages in the perinodal fat. Though the nodes were placed in PBS during transport and washed before imaging, some small blood deposits could have remained leading to a PA signal.

The use of multispectral imaging was however not able to verify that all PA response within the benign nodes could be attributed to hemoglobin, and the spectra did not point to the presence of one specific other chromophore. The fact that the exact blood content and state is unknown in an ex-vivo sample makes it more difficult to verify the exact origin of the signal. In addition, since all samples differ in size and there is a significant variability in the scattering and absorption components between the tissues, it is challenging to compensate for the optical attenuation difference between the wavelengths at different depths within the sample. The APV's normalized for the laser input energy in malignant nodes prove to be higher than those in benign nodes and their drop towards 800 nm seems to be larger. Although the fluence within each sample may have differed, these characteristics could possibly function as additional indicators for metastatic presence. To improve spectral unmixing in future experiments, the implementation of algorithms to correct for light attenuation (26-28) and speed-of-sound inhomogeneities (29), could prove helpful. Further, optical spectroscopy could be used to obtain more knowledge on the exact content of malignant and benign nodal tissue (30).

Next to the use of multi-spectral imaging, anatomical nodal characteristics could possibly be taken into account to increase the distinctive power of the technique. Ultrasound features described as being indicators for metastatic presence, namely increased nodal size, lack of bean shape and the absence of a hilum, could possibly be used to this end. The correlation between measured maximum diameters in the PA images and histology (Table 1) shows that PA is able to produce an accurate depiction of nodal size even when the node is embedded in additional layers of fatty tissue. The PA images (Fig. 2-3) show that all metastatic nodes

measure more than 10 mm while only one of the benign nodes shows an enlarged size. In addition, the contours of two of the malignant nodes seemed more rounded while two of the benign nodes possessed a detectable bean like contour and hilum. The fact that node 2 and 4 lacked a clear nodal outline made the identification of nodal features difficult in these cases which offers some explanation why not all nodes complied with the predictive ultrasound features. Additional imaging using a wavelength of 532 nm could have enhanced these features as we have shown earlier (20). Unfortunately, this excitation wavelength was not available in our present set up but will be taken into account in future experiments. Nodal hilum identification may further be improved by the detection of blood vessels leaving or entering the nodal outline. The use of 800 nm illumination could improve the identification of these structures as shown in Fig. 4. We emphasize that the absence of these features does not fully exclude the possibility of the node harbouring (micro) metastases (31) and these external characteristics can therefore only function as an additional analysis tool.

In general, we can conclude that the detection of melanoma metastases in resected human lymph nodes can be performed using photoacoustics, however a highly accurate parameter to distinguish between malignant and benign nodes is at this point, at the present embodiment of the technique, challenging to define. The amount of PA signal seems to provide an indication for malignancy although the PA signal generated in benign nodes could not be linked to a specific biological chromophore. By paying attention to additional nodal features like shape and size, the distinctive capability of the technique could possibly be increased. Multiple angle illumination could furthermore ensure homogeneous imaging of optically dense or larger samples and application of spectral unmixing algorithms could facilitate a more accurate analysis. To include the use of more excitation wavelengths, we are taking steps towards the implementation of higher sensitivity detectors to reduce the scanning time and the addition of a wavelength-dependent fluence corrections algorithm. A larger photoacoustic study of melanoma metastases will shed more light on the influence of the biological diversity, and the role photoacoustics can play in accurately identifying metastases on the basis of these characteristics.

Acknowledgements

The authors would like to thank the surgical staff of the NKI for their help during the lymph node resections, especially Dr. O. Nieweg. Additionally our thanks go to the Pathological Department of the NKI for sectioning and analyzing the resected nodes, especially to Dr. J. Wesseling.

1. Rigel DS. Epidemiology of melanoma. Semin Cutan Med Surg 2010; 29(4):204-209.
2. Ferlay J, Parkin DM, Steliarova-Foucher E. Estimates of cancer incidence and mortality in Europe in 2008. Eur J Cancer 2010; 46(4):765-781.
3. Edge SB, Compton CC. The American Joint Committee on Cancer: the 7th edition of the AJCC cancer staging manual and the future of TNM. Annals of surgical oncology 2010; 17(6):1471-1474.
4. Breslow A. Thickness, cross-sectional areas and depth of invasion in the prognosis of cutaneous melanoma. Ann Surg 1970; 172(5):902-908.

5. Morton DL, Thompson JF, Cochran AJ, Mozzillo N, Elashoff R, Essner R, Nieweg OE, Roses DF, Hoekstra HJ, Karakousis CP, Reintgen DS, Coventry BJ, Glass EC, Wang HJ. Sentinel-node biopsy or nodal observation in melanoma. N Engl J Med 2006; 355(13):1307-1317.
6. Abe H, Schmidt RA, Sennett CA, Shimauchi A, Newstead GM. US-guided core needle biopsy of axillary lymph nodes in patients with breast cancer: Why and how to do it. Radiographics 2007; 27:S91-S99.
7. van der Velde-Zimmermann D, Schipper MI, de Weger RA, Hennipman A, Rinkes IHMB. Sentinel node biopsies in melanoma patients: A protocol for accurate, efficient, and cost-effective analysis by preselection for immunohistochemistry on the basis of Tyr-PCR. Annals of Surgical Oncology 2000; 7(1):51-54.
8. Wrightson WR, Wong SL, Edwards MJ, Chao C, Reintgen DS, Ross MI, Noyes RD, Viar V, Cerrito PB, McMasters KM, Grp SMTS. Complications associated with sentinel lymph node biopsy for melanoma. Annals of Surgical Oncology 2003; 10(6):676-680.
9. Yao J, Wang LV. Photoacoustic tomography: fundamentals, advances and prospects. Contrast Media & Molecular Imaging 2011; 6(5):332-345.
10. Piras D, Xia W, Steenbergen W, van Leeuwen TG, Manohar S. Photoacoustic imaging of the breast using the twente photoacoustic mammoscope: present status and future perspectives. Selected Topics in Quantum Electronics, IEEE Journal of 2010(99):1-10.
11. Beard P. Biomedical photoacoustic imaging. Interface Focus 2011; 1(4):602-631.
12. Razansky D, Buehler A, Ntziachristos V. Volumetric real-time multispectral optoacoustic tomography of biomarkers. Nat Protoc 2011; 6(8):1121-1129.
13. Telenkov SA, Mandelis A. Photothermoacoustic imaging of biological tissues: maximum depth characterization comparison of time and frequency-domain measurements. J Biomed Opt 2009; 14(4):044025.
14. Grun H, Berer T, Burgholzer P, Nuster R, Paltauf G. Three-dimensional photoacoustic imaging using fiber-based line detectors. J Biomed Opt 2010; 15(2):021306.
15. Nedosekin DA, Sarimollaoglu M, Ye JH, Galanzha EI, Zharov VP. In vivo ultra-fast photoacoustic flow cytometry of circulating human melanoma cells using near-infrared high-pulse rate lasers. Cytometry A 2011; 79(10):825-833.
16. Galanzha EI, Shashkov EV, Kelly T, Kim JW, Yang L, Zharov VP. In vivo magnetic enrichment and multiplex photoacoustic detection of circulating tumour cells. Nat Nanotechnol 2009; 4(12):855-860.
17. McCormack DR, Bhattacharyya K, Kannan R, Katti K, Viator JA. Enhanced photoacoustic detection of melanoma cells using gold nanoparticles. Lasers Surg Med 2011; 43(4):333-338.
18. McCormack D, Al-Shaer M, Goldschmidt BS, Dale PS, Henry C, Papageorgio C, Bhattacharyya K, Viator JA. Photoacoustic Detection of Melanoma Micrometastasis in Sentinel Lymph Nodes. J Biomech Eng-T Asme 2009; 131(7).
19. Jose J, Grootendorst DJ, Vijn TW, Wouters M, van Boven H, van Leeuwen TG, Steenbergen W, Ruers TJ, Manohar S. Initial results of imaging melanoma metastasis in resected human lymph nodes using photoacoustic computed tomography. J Biomed Opt 2011; 16(9):096021.
20. Grootendorst D, Jose J, Van der Jagt P, Van der Weg W, Nagel K, Wouters M, Van Boven H, Van Leeuwen TG, Steenbergen W, Ruers T, Manohar S. Initial experiences in the photoacoustic detection of melanoma metastases in resected lymph nodes. Proc Spie 2011; 7899.
21. Gill KR, Ghabril MS, Jamil LH, Hasan MK, McNeil RB, Woodward TA, Raimondo M, Hoffman BJ, Hawes RH, Romagnuolo J. Endosonographic features predictive of malignancy in mediastinal lymph nodes in patients with lung cancer. Gastrointestinal endoscopy 2010; 72(2):265-271.
22. Catalano MF, Sivak MV, Rice T, Gragg LA, Vandam J. Endosonographic Features Predictive of Lymph-Node Metastasis. Gastrointestinal Endoscopy 1994; 40(4):442-446.

23. Kelly S, Harris K, Berry E, Hutton J, Roderick P, Cullingworth J, Gathercole L, Smith M. A systematic review of the staging performance of endoscopic ultrasound in gastro-oesophageal carcinoma. Gut 2001; 49(4):534-539.
24. Jose J, Willemink RG, Resink S, Piras D, van Hespen JC, Slump CH, Steenbergen W, van Leeuwen TG, Manohar S. Passive element enriched photoacoustic computed tomography (PER PACT) for simultaneous imaging of acoustic propagation properties and light absorption. Opt Express 2011; 19(3):2093-2104.
25. Petrova IY, Petrov YY, Esenaliev RO, Deyo DJ, Cicenaite I, Prough DS. Noninvasive monitoring of cerebral blood oxygenation in ovine superior sagittal sinus with novel multi-wavelength optoacoustic system. Opt Express 2009; 17(9):7285-7294.
26. Rosenthal A, Razansky D, Ntziachristos V. Quantitative Optoacoustic Signal Extraction Using Sparse Signal Representation. Ieee T Med Imaging 2009; 28(12):1997-2006.
27. Shao P, Cox B, Zemp RJ. Estimating optical absorption, scattering, and Grueneisen distributions with multiple-illumination photoacoustic tomography. Appl Opt 2011; 50(19):3145-3154.
28. Jetzfellner T, Razansky D, Rosenthal A, Schulz R, Englmeier KH, Ntziachristos V. Performance of iterative optoacoustic tomography with experimental data. Appl Phys Lett 2009; 95(1).
29. Schoonover RW, Anastasio MA. Image reconstruction in photoacoustic tomography involving layered acoustic media. J Opt Soc Am A Opt Image Sci Vis 2011; 28(6):1114-1120.
30. Kanick SC, van der Leest C, Djamin RS, Janssens AM, Hoogsteden HC, Sterenborg HJCM, Amelink A, Aerts JGJV. Characterization of mediastinal lymph node physiology in vivo by optical spectroscopy during endoscopic ultrasound-guided fine needle aspiration. Journal of Thoracic Oncology 2010; 5(7):981.
31. Catalano MF, Sivak Jr MV, Rice T, Gragg LA, Van Dam J. Endosonographic features predictive of lymph node metastasis. Gastrointestinal endoscopy 1994; 40(4):442-446.

Table 1. Lymph node sizes

#	Maximum diameter in histology (mm)	Maximum diameter in PA image (mm)
1	17	15
2	17	17
3	20	20
4	9	7
5	10	11
6	6	7

Table 2. Photoacoustic imaging parameters

#	Energy (mJ/cm^2)*	Wavelengths (nm)▪	Projections●
1	30	720-760-800	20
2	30	720-740-760-780-800	20
3	40	720-740-760-780-800	40
4	25	720-760-800	20
5	25	720-760-800	20
6	25	720-760-800	20

* Energy was varied depending on the size of the node

■ Additional excitation wavelengths were used to more accurately define the PA response of the different structures within the node

● Additional projections were taken depending on the quality of the image

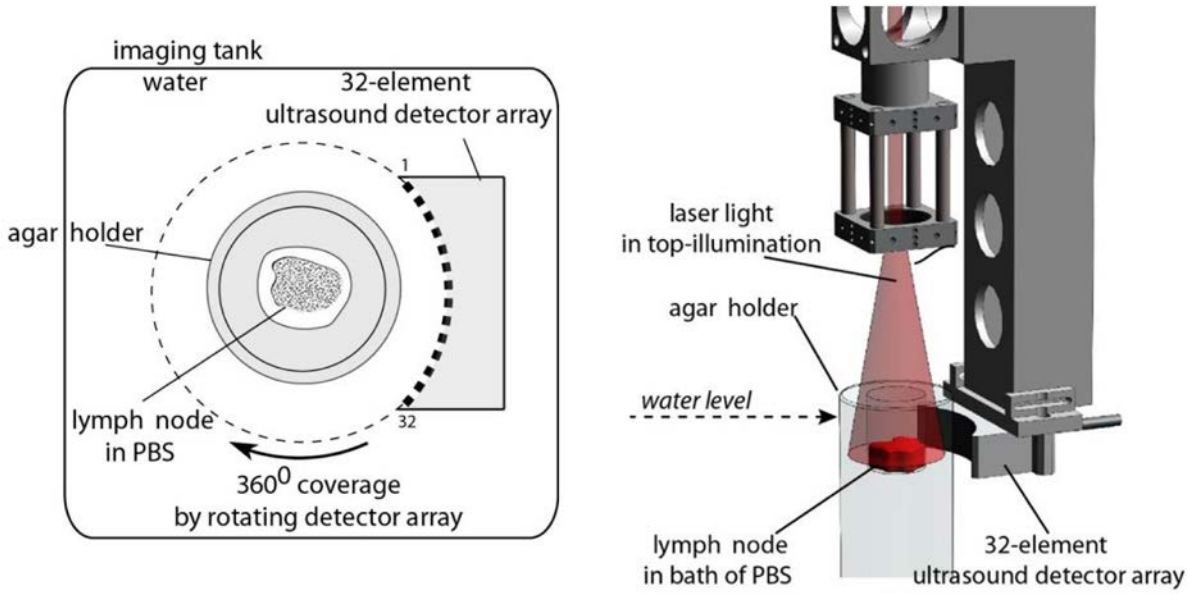

Fig. 1. Tomographic PA setup utilizing top illumination. The holder containing the lymph node is illuminated from the top while the ultrasound detector is rotated around the holder. Reproduced from Ref. 19 with permission from the authors and SPIE.

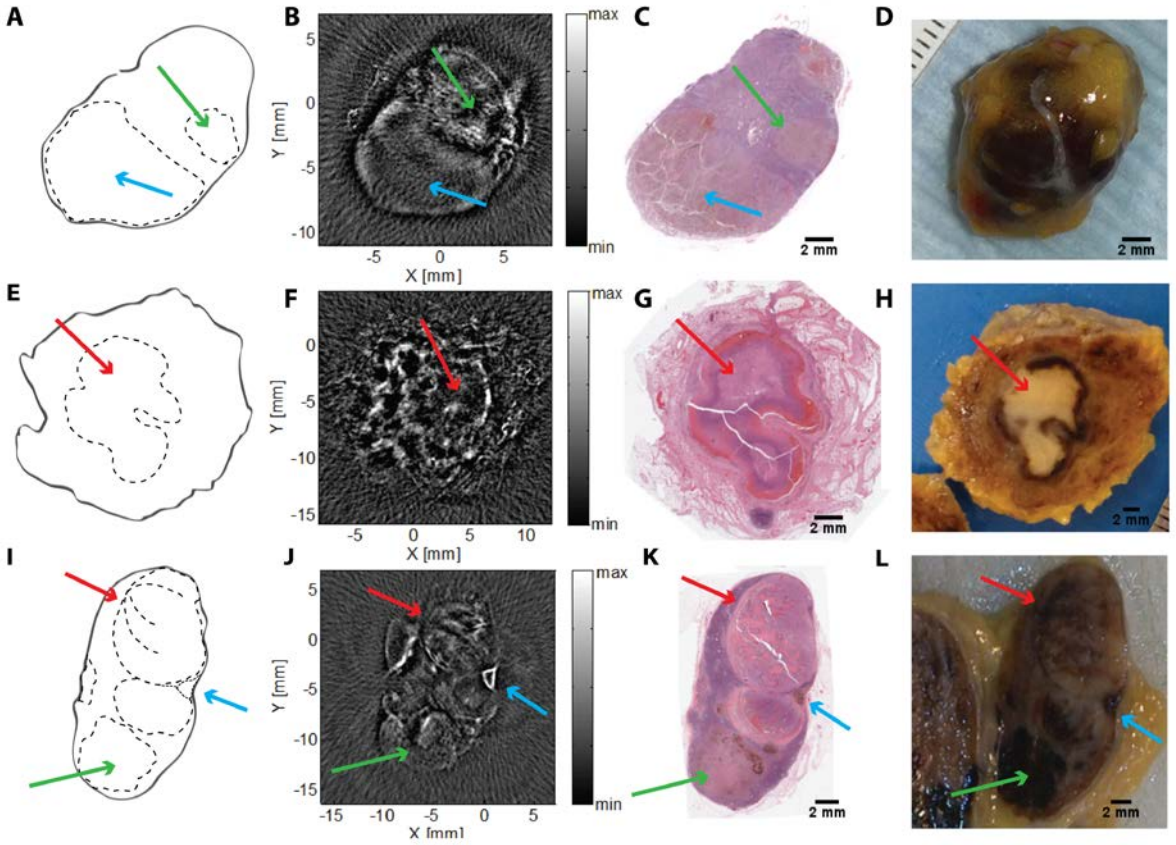

Fig. 2. PA images of malignant nodes at 720 nm. Color scales are optimized to display the identified features. A, E, and I: Layout of the visualized structures within each node based on contour of the histopathological images (C, G, and K). B: PA image of lymph node 1.Contrast is increased throughout the upper part of the node and a small area around 2 O'clock shows an increased response (green arrow). C: Corresponding pathological slice. Melanoma cells present throughout the node, especially at 2 O'clock and 7 O'clock. D: Corresponding

photograph of unsliced node. F: PA image of lymph node 2. Slice shows a ring of increased contrast located around the unenhanced centre of the node (red arrow). G: Corresponding pathological slice. Melanoma cells are located around a necrotic centre (red arrow) H: Corresponding photograph of the sliced node before staining. Diffuse darkening of the nodal volume which contains a large necrotic area surrounded by a dark ring of melanoma cells (red arrow). J: PA image of lymph node 3. A small triangle of increased response is located at 3 O'clock (blue arrow) and some ring like response patterns can be distinguished at 12 O'clock (red arrow). K: Corresponding pathological slice showing a triangular melanin rich area at 3 O'clock (blue arrow) and some additional vital melanoma cells in curved patterns grouped around and throughout the necrotic center at 12 O'clock (red arrow). L: Corresponding photograph of the sliced node before staining. Dark triangular area at 3 O'clock is distinguishable (blue arrow) and ring like patterns in the upper part of the node are visible (red arrow).

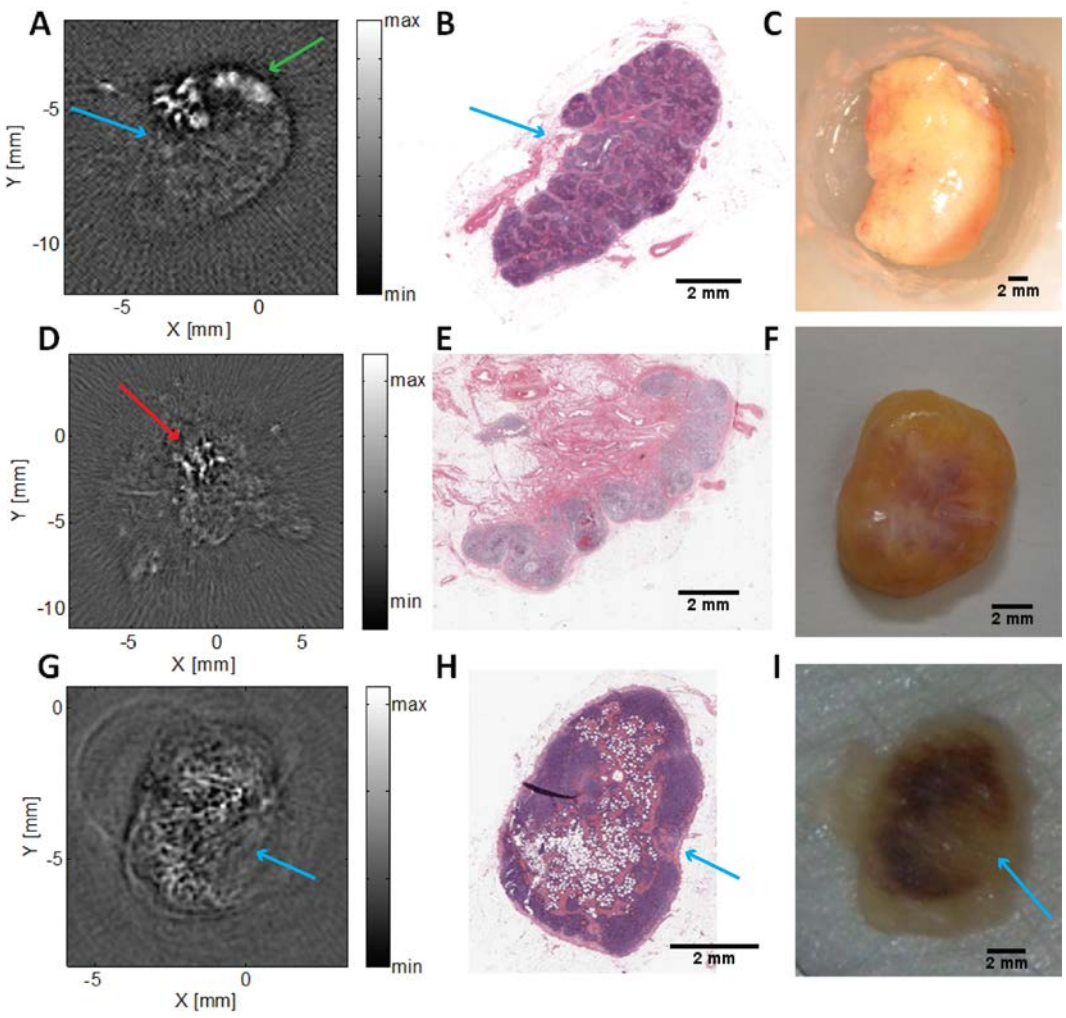

Fig. 3. PA images of benign nodes at 720 nm. Color scales are optimized to display the identified features. A: PA image of lymph node 4. Contrast is increased in the upper part of the node (green arrow) and a slight notch indicating the hilum can be seen at 10 O'clock (blue arrow). B: Corresponding pathological slice. Hilum location correlates to PA image (blue arrow). C: Corresponding photograph of unsliced node. D: PA image of lymph node 5. Slice shows a speckle pattern which is most intense in the centre of the image (red Arrow). E: Corresponding pathological slice. F: Corresponding photograph of unsliced node. G: PA image of lymph node 6. Notch around 4 O'clock resembles hilum location (blue arrow). H: Corresponding pathological slice showing hilum location (blue arrow). I: Corresponding photograph of the sliced node before staining. Darkening throughout the tissue resembles PA shape. Hilum is located at 4 O'clock (blue arrow).

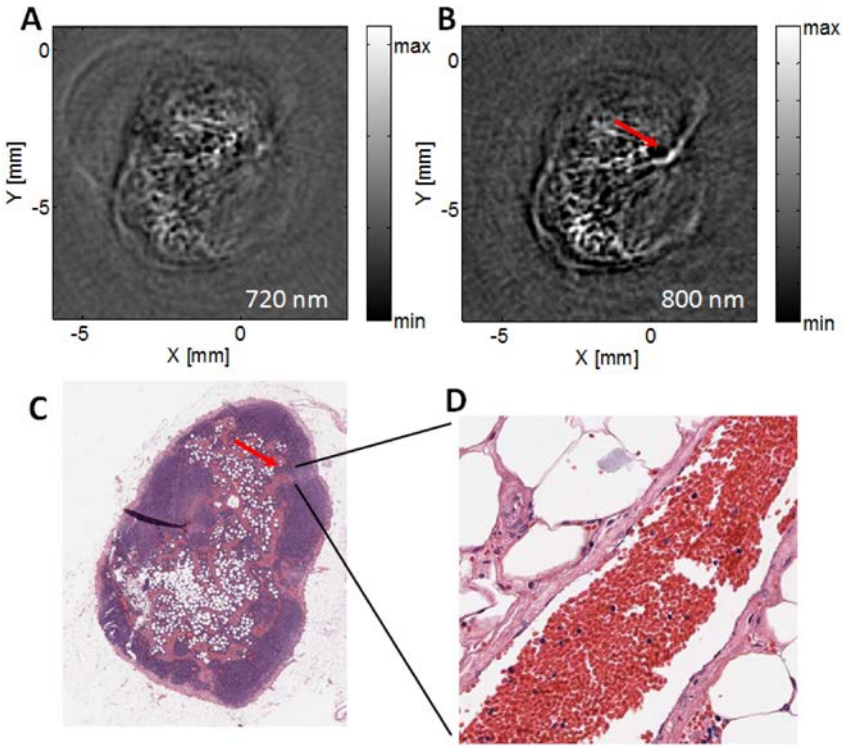

Fig. 4. A: Lymph node 6. Map of the PA response within the lymph node at 720 nm. PA response is present throughout the node, however no vessel like structures are visible. B: Map of the PA response within the lymph node at 800 nm. PA response is present throughout the node and a vessel like structure is located in the upper right (red arrow). C: Pathological overview of the node. Slice shows a fatty node without malignant cells. D: Amplification reveals red blood cells in a small vessel exiting the node boundary.

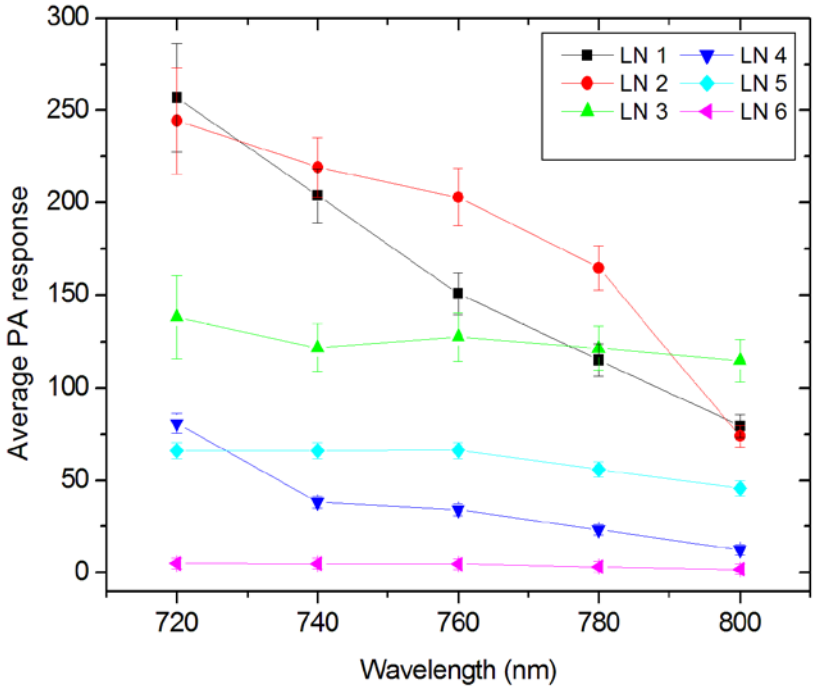

Fig. 5. Average pixel values (APVs) of the selected areas within the lymph nodes (LN) at different illumination wavelengths.